FEATURE ARTICLE

Nanophotonics: Interactions, Materials, and Applications

Yuzhen Shen, Christopher S. Friend, Yan Jiang, Daniel Jakubczyk, Jacek Swiatkiewicz, and Paras N. Prasad*

Photonics Research Laboratory, Institute for Lasers, Photonics and Biophotonics, Departments of Chemistry, Physics and Electrical Engineering, State University of New York at Buffalo, Buffalo, New York 14260

Received: April 26, 2000; In Final Form: June 9, 2000

This article presents our comprehensive study in the new area of nanophotonics, which deals with optical processes at the nanoscale, much smaller than the wavelength of optical radiation. Nanoscale matter−radiation interactions, which include nanoscale confinement of radiation, nanoscale confinement of matter, and nanoscale photophysical or photochemical transformation, offer numerous opportunities for both fundamental research and technological applications. We present here selected examples of our studies in each of these areas. Nonlinear optical interactions involving nanoscale confinement of radiation are theoretically analyzed and experimentally probed using a near-field geometry. Nanoscale confined optical domains to control excitation dynamics and energy transfer and to produce photon localization are illustrated by examples of nanostructured rare-earth-doped glasses, multiphasic nanocomposites, and photonic band gap materials. One application of nanophotonics presented here is the utilization of spatially localized photochemistry using a near-field excitation for nanofabrication and nanoscale memory. The article concludes with a discussion of the future outlook for nanophotonics.

I. Introduction

Nanophotonics is a new frontier that describes nanoscale optical science and technology. It offers challenging opportunities for studying fundamental processes of interaction between the radiation field and matter on a scale much smaller than the wavelength of radiation. Furthermore, the use of such confined interaction to spatially localize photochemical processes also offers exciting opportunities to chemists. Nanophotonics is of considerable technological significance. As a matter of fact, nanophotonics has already made its impact on new technologies. Quantum well lasers and quantum cascade lasers are examples which utilize nanoscale optical processes. Even at the consumer goods level, TiO_2 nanoparticles are used in sunscreen lotions as effective UV radiation blockers.

This article describes our program in nanophotonics, highlighting some selected results. In our program, nanophotonics is divided into three sections as shown in Table 1.

I.A. Nanometer Confinement of Radiation. Conventional optical studies have been conducted in the far-field. Due to the diffraction limit of the probe light, the information obtained is the average response over a macroscopic region. The near-field scanning optical microscopy (NSOM)[1−6] and photon scanning tunneling microscopy (PSTM)[7−12] overcome this diffraction limit and make it possible to probe localized optical interactions in nanoscopic regions. The principle of NSOM is to scan a nanoscopic light source in the near-field above a sample with the resulting field intensity being detected. With PSTM, a nanoscopic probe senses the evanescent field above a sample that is illuminated under total internal reflection. The optical processes detected by NSOM and PSTM involve both a propagating field (also called allowed light which has its wave vector real) and an evanescent field (also called forbidden light where the wave vector is imaginary).[13−15] However, most efforts related to NSOM and PSTM have concentrated on linear optical effects,[16−34] the area of nonlinear optical interactions at nanometer scale is still virtually unexplored.[35−44] The latter is the focus of work being conducted in our laboratory.

I.B. Nanometer Confinement of Matter. Multifunctional composite materials that simultaneously exhibit more than one property are a new generation of materials which hold considerable promise for numerous applications in the field of electronics and photonics.[45] Nanosize manipulation of molecular architecture and morphology provide a powerful approach to control the electronic and optical properties of a material as well as its processability. In recent years, the design and processing of nanostructured materials have emerged as a frontier area of material research. The electronic and photonic properties of these materials are strongly dependent on their band gaps. Band-gap dependence has been well documented in the case of inorganic semiconductors, where nanostructure quantum dots of different sizes have been used to control the electronic, luminescence, and nonlinear optical properties.[46−51] Furthermore, nanosize control of the local structure also provides an opportunity to manipulate excitation dynamics by controlling the local phonon density of states as well as to influence energy transfer by controlling intermolecular interactions.

I.C. Nanoscale Photoprocesses for Nanofabrication. The recent increasing interest in photoprocesses is driven by the future needs of industrial applications, including integrated

* Corresponding author.

10.1021/jp0016131 CCC: $19.00
Published on Web 07/15/2000

TABLE 1

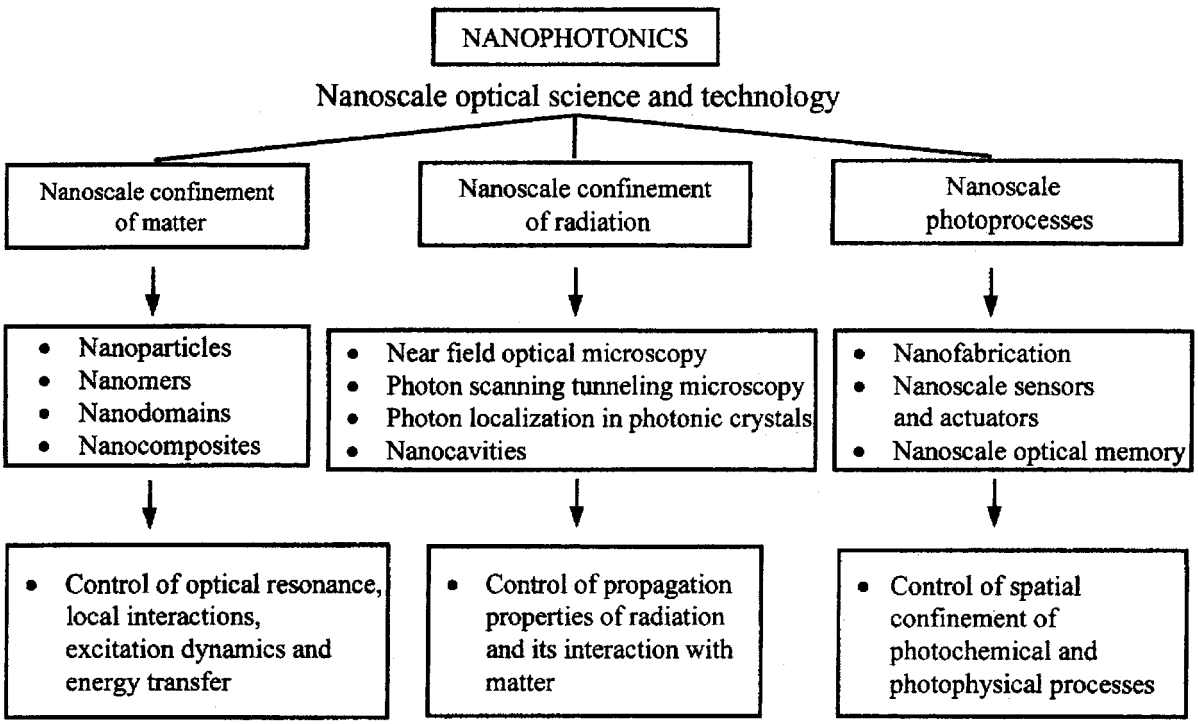

circuit designs, integrated optoelectronic coupling, surface treatment, data storage, and lithography. These applications require a significant improvement in photosensitive technology with a higher degree of precision and resolution. The spatial resolution in a conventional photoprocessing device depends on the spot size of the light source, which is diffraction-limited. Thus, the transverse size of the produced structure is close to the submicron level. The near-field optical technique overcomes the diffraction-limited spot size, offers advantages over the conventional photoprocessing technique in precision and fine resolution, and extends the capability of photoprocessing to the nanometer region. Although the applications of NSOM are still limited, definite progress has been made recently in the areas of photoprocessing and photofabrication.[52−57]

This article presents our recent studies in these three areas of nanophotonics, with a special emphasis on nonlinear optical interactions. In Section II, we first present our theoretical modeling of nanoscale nonlinear optical interactions, specifically second-order effects. This work utilizes a combination of the multiple-multipole model and nonlinear coupled wave equations. We then describe our experimental studies on nanoscale nonlinear optical imaging and second harmonic generation using the near-field optical technique. In Section III, we present selected examples of our work on nanostructured materials to control optical interactions and excited-state dynamics. We present three examples: (i) rare-earth-doped nanostructured glasses in which the excited-state dynamics are controlled to achieve efficient emission; (ii) nanostructured multiphasic composites in which the energy transfer between domains is controlled to achieve multiwavelength lasing; and (iii) photonic band gap materials which exhibit localization of photons of certain wavelength. In Section IV, we describe our work on nanofabrication and nanoscale optical memory. Section V provides some future outlook for nanophotonics.

II. Interactions

II.A. Theoretical Modeling of Nanoscale Second-Order Optical Interactions. For a rigorous theoretical description of nanoscale optical interactions, both the near- and the far-fields have to be considered simultaneously with objects ranging from subwavelength to several wavelengths in size. Therefore, it is necessary to solve the complete wave vector equations. Analytical solutions of Maxwell's equations can provide a good theoretical understanding of simple problems; a purely numerical approach can be applied to complex structures but is limited in size by computational requirement. The multiple-multipole (MMP) model[58,59] is a compromise between a purely analytical and a purely numerical approach, which can be used for solving Maxwell's equations for arbitrarily shaped, isotropic, linear, and piecewise homogeneous media. With the MMP model, the electromagnetic field $f \in \{E, H\}$ within individual domains D_i is expanded by analytical solutions of Maxwell's equations:

$$f^{(i)}(\mathrm{r}, \omega_0) \approx \sum_j A_j^{(i)} f_j(\mathrm{r}, \omega_0) \tag{1}$$

The basic function $f_j(\mathbf{r}, \omega_0)$ satisfies the wave vector equation for the eigenvalue q_j

$$-\nabla \times \nabla \times f_j(\mathbf{r}, \omega_0) + q_j^2 f_j(\mathbf{r}, \omega_0) = 0 \tag{2}$$

The parameters $A_j^{(i)}$ of the series expansions are numerically matched on the interfaces. Consequently, Maxwell's equations are exactly fulfilled inside the domains; however, they are only approximated at the boundaries.

The main characteristics of nonlinear optics in the near-field is that it does not need to fulfill the usual phase matching condition as the domains are much smaller than the coherence length. Starting from Maxwell's equations, the electric fields of the fundamental and the second-harmonic (SH) waves are satisfied by the nonlinear coupled wave equations[60]

$$\nabla \times \nabla \times \mathbf{E}(\mathbf{r}, \omega_0) - \frac{\omega_0^2}{c^2}\epsilon(\mathbf{r}, \omega_0)\mathbf{E}(\mathbf{r}, \omega_0) = 4\pi\frac{\omega_0^2}{c^2}\mathbf{P}^2(\mathbf{r}, \omega_0) \tag{3}$$

$$\nabla \times \nabla \times \mathbf{E}(\mathbf{r}, 2\omega_0) - \frac{4\omega_0^2}{c^2}\epsilon(\mathbf{r}, 2\omega_0)\mathbf{E}(\mathbf{r}, 2\omega_0) = 4\pi\frac{\omega_0^2}{c^2}\mathbf{P}^2(\mathbf{r}, 2\omega_0) \quad (4)$$

where $\epsilon(\mathbf{r}, \omega_0)$ and $\epsilon(\mathbf{r}, 2\omega_0)$ are the linear dielectric functions for the fundamental and the SH waves, respectively.

Since the conversion efficiency from the fundamental wave to the SH wave is relatively low, the electric field intensity of the fundamental wave is assumed to be unchanged. The nonlinear material employed in our calculation is the *N*-(4-nitrophenyl)-(L)-prolinol (NPP) nanocrystal, for which all nonlinear coefficients except d_{21} and d_{22} are negligible.[61] The nonlinear polarization $\mathbf{P}^{(2)}(\mathbf{r}, 2\omega_0)$ can then be written as

$$P_x^{(2)}(\mathbf{r}, 2\omega_0) = 2d_{21}E_x(\mathbf{r}, \omega_0)E_y(\mathbf{r}, \omega_0) \quad (5)$$

$$P_y^{(2)}(\mathbf{r}, 2\omega_0) = d_{21}E_x(\mathbf{r}, \omega_0)E_x(\mathbf{r}, \omega_0) + d_{22}E_y(\mathbf{r}, \omega_0)E_y(\mathbf{r}, \omega_0) \quad (6)$$

Now consider a plane wave that tunnels from a medium of refractive index n1 through a vacuum gap and into a medium of refractive index *n*2, where $n2 < n1$. Assuming the electrical field from the probe is $\mathbf{A}_0(\mathbf{k}_{||})$, where $\mathbf{k}_{||} = (k_x, k_y)$, the corresponding electrical field at the sample surface is

$$\mathbf{E}_s(\mathbf{k}_{||}) = \boldsymbol{A}_0(\mathbf{k}_{||}) \exp(i\mathbf{k}_{||}\mathbf{r}_{||}) \exp(ik_z d) \quad (7)$$

where $\mathbf{r}_{||} = (x, y)$, *d* is the probe-sample distance, and

$$k_z = (\mathbf{k}^2 - \mathbf{k}_{||}^2)^{1/2} = k_0(1 - n_1^2 \sin^2\theta)^{1/2} \quad (8)$$

in which $k_0 = 2\pi/\lambda$, λ is the wavelength of light in free space, n_1 is the refractive index of the probe, and θ is the incident angle. If $1 - n_1^2 \sin^2\theta$, i.e., k_z is real, the waves will propagate with a constant amplitude between the probe and the sample, which corresponds to the allowed light in the sample. When k_z is imaginary, the waves will decay exponentially within distances comparable to the wavelength, and such waves are called the evanescent waves, which produce the forbidden light in the sample. Therefore, from the electrical field distribution of the fundamental wave calculated with the MMP method, we can obtain the electrical field distribution of the SH wave and the different contributions of allowed light and forbidden light to the SH wave.

Figure 1 shows the near-field intensity distribution of the fundamental wave and the SH wave in the $X-Y$ plane (parallel to the surface of the sample) and $X-Z$ plane (perpendicular to the surface of the sample), respectively. Unlike the forbidden light, the allowed light is more localized at the center of the tip. With the gap width increasing, the field intensity from the forbidden light decreases dramatically and the field intensity from the allowed light dominates. From Figure 2b,c we can conclude that the field intensity of the SH wave is highly localized in both the lateral and the vertical dimensions within the probe center, i.e., about 50 nm × 50 nm. Therefore, near-field imaging with SHG could provide better resolution.

Figure 2 shows the sectional plot of Figure 1 along the *x*-axis, and Figure 3 shows the integration of $|E|^2$ for the SHG over the total solid angles. It is clear that the field intensity close to the probe center comes from the allowed light, while a field enhancement appears at the edge of the probe due to significant contribution from the forbidden light. The field intensity decreases very rapidly with the probe-sample distance and its typical decay length is comparable to the tip size, i.e., about 50 nm. Furthermore, the field intensity of the forbidden light, which decays exponentially, exhibits a much faster variation with the probe-sample distance than does the field intensity of the allowed light. Figure 3 also indicates that, when the probe is

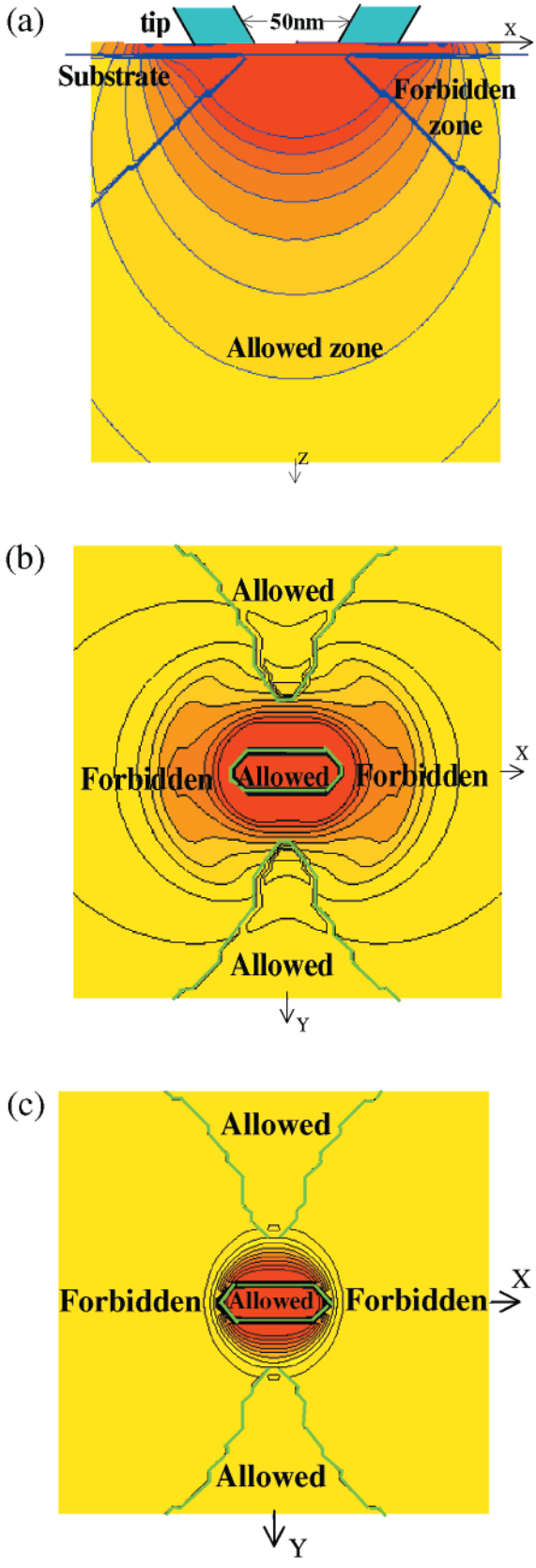

Figure 1. Optical near-field intensity distribution of the fundamental wave in the $X-Z$ plane (a) and in the $X-Y$ plane (b) and of the second harmonic generation in the $X-Y$ plane (c) for 50 nm apertured Al-coated tapered fiber.

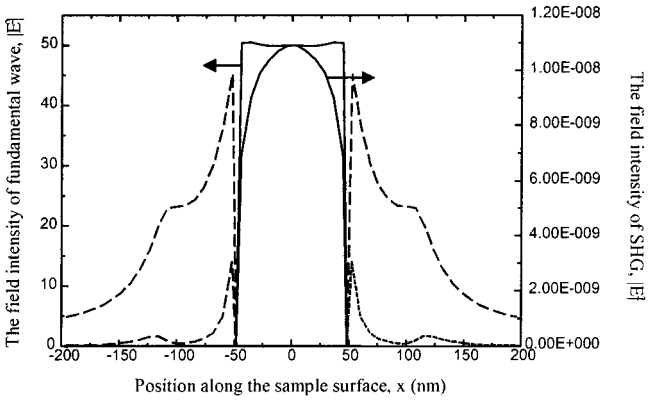

Figure 2. The electrical field intensity of the fundamental wave and the second harmonic generation along the sample surface for several different probe−sample distances. (Solid curve: field intensity of allowed light; dashed curve: field intensity of the forbidden light.)

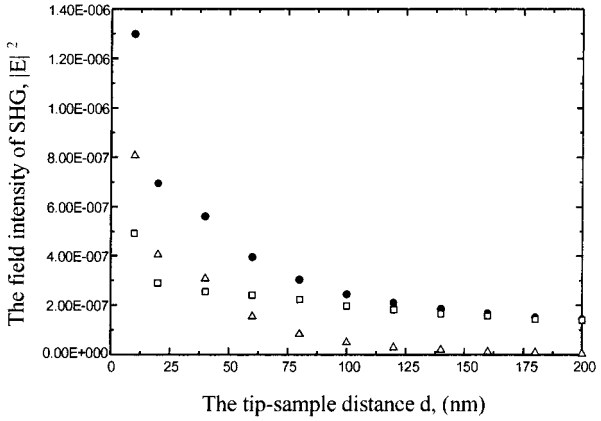

Figure 3. The effect of the tip−sample distance *d* on the near-field intensity of the SHG from the total field (solid circle), allowed light (open square), and forbidden light (open triangle).

very close to the sample surface, $d < 50$ nm, relative to the probe size, the intensity from the forbidden light dominates. However, when the probe-sample distance is larger than 50 nm, the intensity from the allowed light becomes the main contribution to the total field intensity. Because the allowed light carries only the information with low spatial frequencies, the detection of the forbidden light is essential to improve the resolution of the image obtained.

Figure 4 shows the effect of the polarization direction of the incident wave on the near-field intensity, assuming φ is the angle between the normal of the incident plane, i.e., the *y*-axis and the electric field vector of incident light. Thus $\varphi = 0°$ corresponds to the s-polarization of the fundamental wave, whereas $\varphi = 90°$ to the p-polarization state. Figure 4 indicates that the near-field intensity also depends on the polarization angle φ of the incident wave. When $\varphi > 45°$, the p-polarization component in the near-field intensity of the fundamental wave is overwhelming. The *z*-component of the incident field dominates, and the field intensity decreases gradually with increasing polarization angle φ. When $\varphi < 45°$, the s-polarization component overwhelms, the field intensity increases rapidly with the polarization angle φ due to an increase of the *y*-component in the incident field. However, for the second harmonic wave, the turning point shifts to $\varphi = 55°$ due to the relative magnitudes of the d_{21} and d_{22} coefficients.

II.B. Nanoscale Nonlinear Optical Imaging. Two-photon excitation microscopy is a nonlinear optical imaging technique which has the advantages of effective rejection of background,

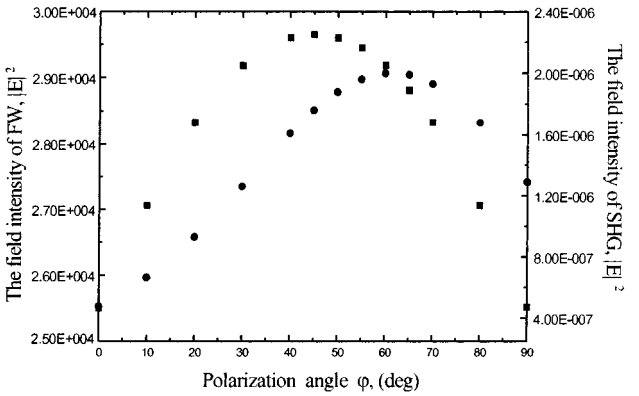

Figure 4. The dependence of the near-field intensity on the polarization direction of the incident light. (Solid square: field intensity of the fundamental wave; solid circle: field intensity of the second harmonic wave.) The calculation is performed with the probe−sample distance of 10 nm.

reduced volume of photobleaching, and depth discrimination.[62] Some of these advantages can benefit NSOM and PSTM. We have extended femtosecond two-photon excitation to both NSOM[39] and PSTM.[40] The schematic diagrams of two-photon NSOM and PSTM are shown in Figure 5a,b, respectively, and both setups are developed on the basis of a commercial NSOM instrument (Topometrix, Lumina).

For two-photon NSOM, a self-mode-locked Ti:sapphire laser is used as an excitation source at 800 nm with an average power of 1.5 mW. The laser light is coupled into a 1-m single-mode optical fiber and illuminates the sample through an aluminum-coated probe with an aperture of 50 nm, as shown in Figure 5a. Dispersion induced by the optical fiber is compensated by a 350 line/mm grating pair. ZnS:Mn nanoparticles with a diameter of 150−250 nm and encapsulated with 2-{4-{(ϵ)-2-{4-(sulfonyl)phenyl}-1-ethenyl}(methyl) anilino]-1-ethanethiol (APSS-SH) were imaged. APSS-SH is a new efficient two-photon upconvertor prepared in our laboratory, which contains a thiol terminated group that chemically bonds to the surface of a ZnS:Mn particle. Figure 6 shows the near-field two-photon fluorescence image of APSS-SH/ZnS:Mn particles, in which a feature at the full-width at half-maximum (fwhm) of 240 nm is obtained, consistent with the particle size. The improved resolution of two-photon excitation is due to the quadratic dependence of two-photon excitation, which limits the effective excitation to a small volume at the aperture of the probe and enhances the light confinement.

Due to the enhanced light confinement, the two-photon NSOM can also effectively reject the background from the illuminated zone and improve the image contrast. However, it is found that the nonlinear emission in the fiber overlaps with the fluorescence from the specimen and contributes to the background.[39,42,43] Furthermore, although a pulse compressor can compensate for the group-velocity dispersion induced by the fiber, the nonlinear effect such as self-phase modulation is not easily corrected.[43] To suppress the background signal and improve the image contrast, a metal tip illuminated with a femtosecond laser has been utilized as a localized excitation source to generate a strongly enhanced electric field at the metal tip for two-photon imaging in NSOM. A signal-to-noise ratio of better than 10:1 has been obtained.[63]

Our recent studies have demonstrated that two-photon PSTM can provide advantages in signal-to-noise improvement and in system alignment compared to two-photon NSOM. The same self-mode-locked Ti:sapphire laser is used as an excitation source with an average power of 12 mW for two-photon PSTM.

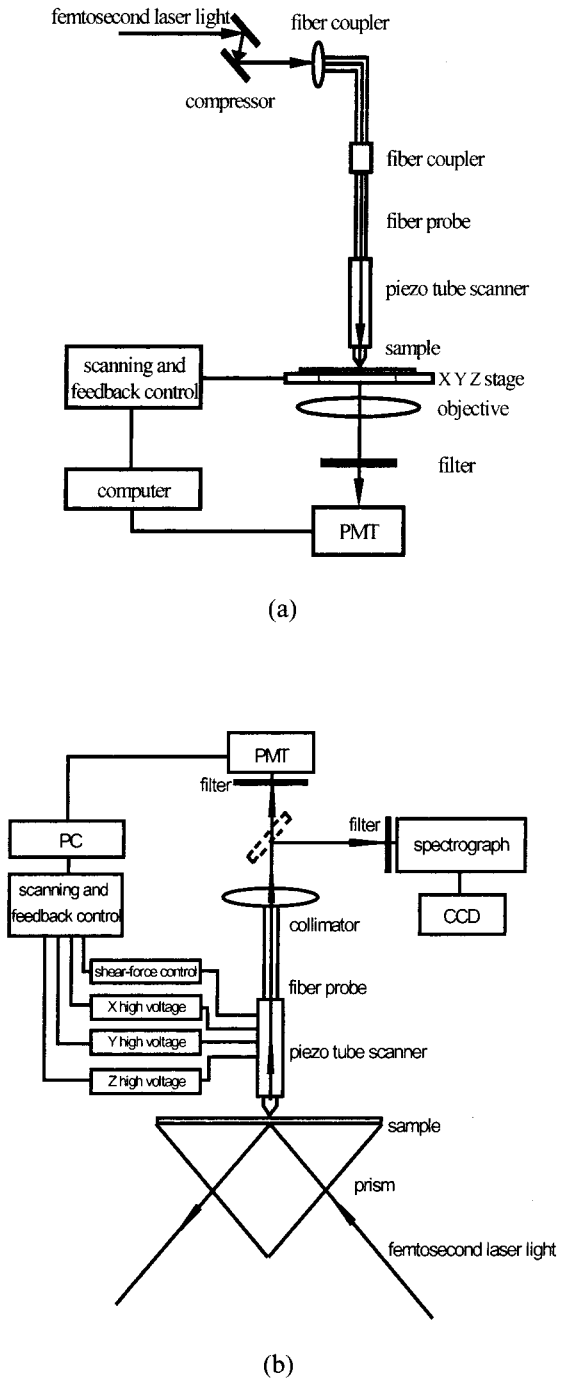

Figure 5. Schematic of two-photon near-field scanning optical microscopy and photon scanning tunneling microscopy.

The laser beam is focused by a lens and illuminates the sample that is mounted with an index matching oil on a fused silica prism under total internal reflection, as shown in Figure 5b. The dispersion length is only 5 mm, and pulse broadening and nonlinear effects are negligible. The measurement of both intensity dependence and spectral dependence is performed on a two-photon chromophore (AF-390) that was synthesized at the Polymer Branch of the U.S. Air Force Research Laboratory. Figure 7a shows the near-field two-photon fluorescence image, and the fwhm of the optical intensity profile is 340 nm. It is interesting to note that the emission patterns in the fluorescence image are oriented in the same direction for all isolated particles. Such an effect is mostly due to the polarization-dependent dipolar interaction.[64] Since the incident light is linearly polarized, once excited, the molecules act as electric dipoles and dipole

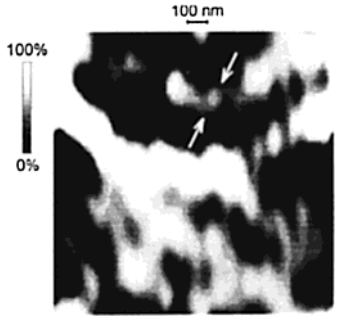

Figure 6. Two-photon fluorescence NSOM image of APSS-SH/ZnS: Mn nanoparticles

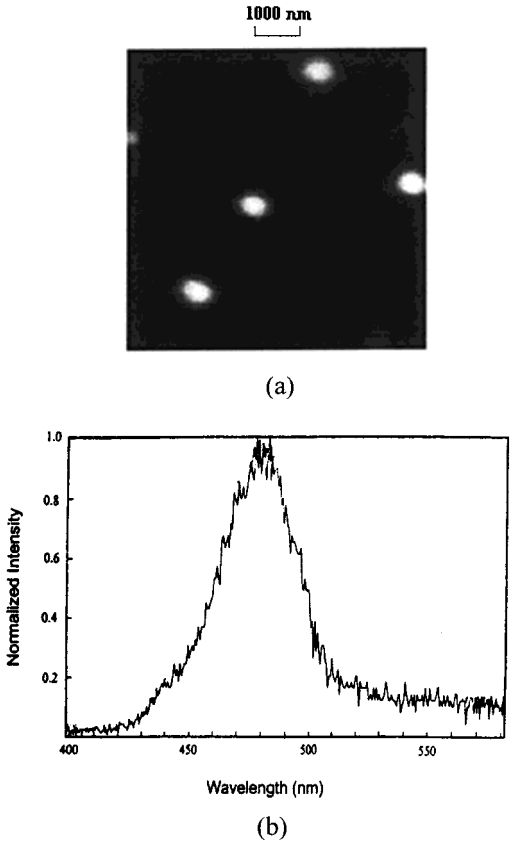

Figure 7. (a) Two-photon fluorescence PSTM image of a AF-390 nanoparticle. (b) Near-field fluorescence spectrum of a AF-390 nanoparticle (acquisition time: 90 s).

orientations approximately follow the excitation polarization. Therefore, the spatial fluorescence feature indicates the high degree of molecular order in the isolated nanoparticles. This can be further demonstrated by the near-field fluorescence spectrum of isolated AF-390 nanoparticles as shown in Figure 7b. The spectrum exhibits a slight shift relative to the bulk spectrum (not shown), and is narrower. This is due to the fact that an isolated nanoparticle exists in a highly organized state with a high degree of molecular order and a small energy distribution, which leads to spectral line narrowing.[65,66] With two-photon excitation, the quadratic dependence of two-photon excitation on light intensity enables a light confinement at the aperture of the probe, and enhances the image contrast with a coated probe, as can be clearly seen in Figure 7a.

Since the evanescent field decays exponentially, the depth of penetration for PSTM is limited.[67] However, two-photon PSTM still provides some advantages in reduced alignment constraints and minimized background interference, and shows potential benefit in thin film analysis.

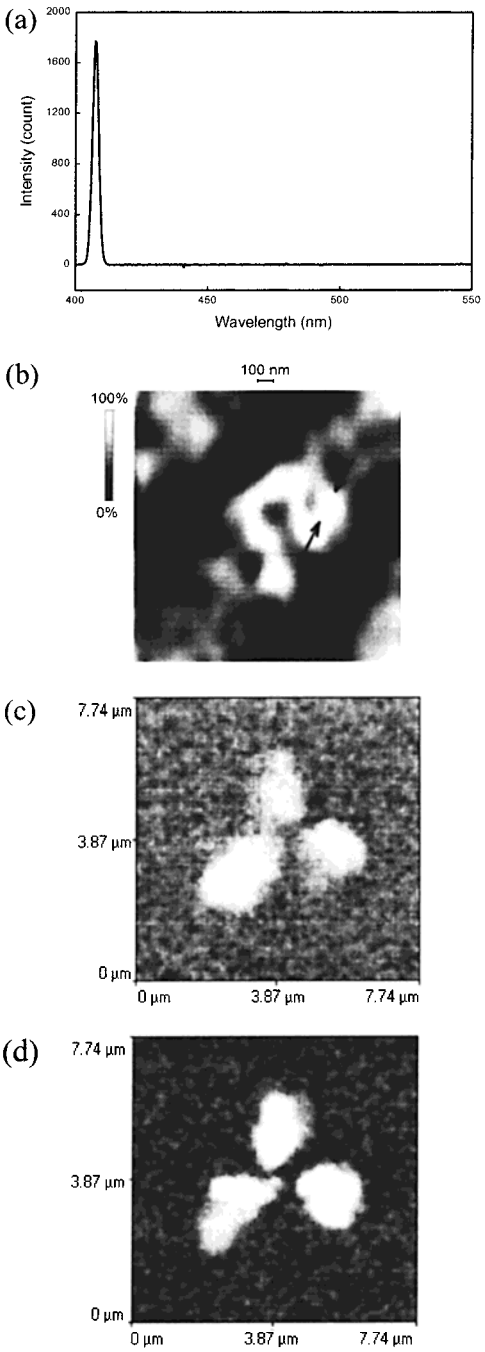

Figure 8. (a) Near-field SHG spectrum, (b) image of NPP nanocrystals, (c) and (d) SHG in NPP crystals for two orthogonal polarizations.

II.C. Nanoscale Second-Harmonic Generation (SHG). Since second-harmonic generation (SHG) is known to be surface sensitive on the atomic scale,[36] it is possible to study localized nonlinearity by near-field probing of SHG. The experimental setup in our studies is the same as in Figure 1a, and NPP nanocrystals are used as the sample because of the high second-order susceptibility. We observed that the background emission induced in the fiber decreases considerably for wavelengths below 500 nm. Thus, SHG from an 800 nm fundamental wave can also utilize this signal-to-noise improvement, and it can be clearly seen in the near-field SH spectrum of NPP nanocrystals, as shown in Figure 8a. Since the coherence length for SHG in a NPP crystal at 800 nm is expected to be of the order of at least several micrometers, considerably larger compared with NPP nanoparticles, the fields from different NPP molecules within a crystallite always add constructively (coherence limit phase matching). Figure 8bshows the SH image of NPP nanocrystals, in which the objects as small as 140 nm can be distinguished. The highly localized SH intensity distribution is consistent with our theoretical simulation. Further studies indicate that the image contrast of the localized SH field is polarization-dependent, as shown in Figure 8c,d.

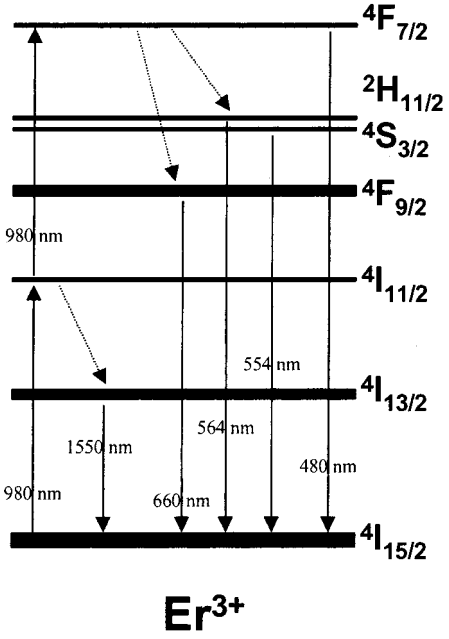

Figure 9. Schematic diagram of energy levels and transitions of Er^{3+}-doped system.

Similar SHG studies have been conducted by other groups on Langmuir−Blodgett (LB) film,[38] lead zirconate titanate piezoceramic,[35] and a silver surface,[36] and the results also demonstrated a localized nonlinear response at the nanometer scale.

III. Materials

Nanoscale confinement of matter can be used to control the band gap and the optical resonance as well as to control the excitation dynamics. Furthermore, an even more exciting new area is use of nanoscale confinement to produce periodic optical domains that lead to photon localization. We are actively pursuing all of these directions.

Nanoscale confinement of domains to produce quantum dots, quantum wells, and quantum wires in inorganic semiconductors is well-known and extensively studied.[68] In our laboratory, we have extended this concept to nanomers of π-conjugated structures. We have shown that using reverse micelle chemistry, oligomeric structures with well-defined π-electron delocalization lengths can be produced.[69] Thus, optical resonance ($\pi \rightarrow p^*$ transition) in these structures can be judiciously selected.

In this paper we provide three selected examples of nanoscale confinement of matter to control excitation dynamics and energy transfer and to produce photon localization.

III.A. Nanostructured Rare-Earth-Doped Glasses. A nanostructured rare-earth-doped glass is chosen as an example of a material with controlled excitation dynamics. The rare-earth ions have received a great deal of attention both for their ability to exhibit a wide range of radiative properties and for their application as lasing and amplifying media.[70] An example is an Er^{3+}-doped system. Its energy level structure and various possible radiative, and nonradiative transitions are shown schematically in Figure 9. The major prominent radiative process is the emission ($^4I_{13/2} \rightarrow {}^4I_{15/2}$ transition) which has been used

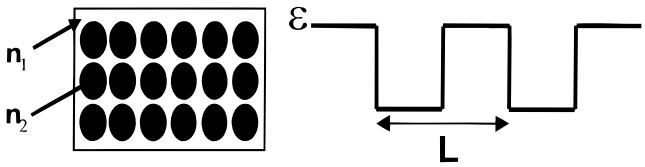

Figure 10. Basic structure of a photonic crystal.

for optical amplification in telecommunication. Er^{3+} also shows a very efficient up-converted emission ($^4S_{3/2} \rightarrow {}^4I_{15/2}$ transition) when pumped at 980 nm. The efficiencies of these processes are determined by the excitation dynamics of the pumped level which is governed by the local phonon density of states and coupling of the various intermediate levels to the lattice. A low-frequency phonon lattice helps reduce the nonradiative process and enhance the radiative process. Also, new channels of nonradiative processes known as concentration quenching come into play if ion clustering takes place at higher Er^{3+} concentration levels.

Silica glasses have been used as a high-quality optical media, but depending on the method of preparation, they may contain different amounts of hydroxyl groups that have a high phonon frequency mode and can be an efficient quencher.

We have developed methods using a variation of the sol−gel technique, in which the local environment of the rare-earth ion Er^{3+} consists of a low-frequency phonon crystalline medium to reduce the nonradiative processes. This method has yielded a lifetime of 18 ms for the 1.55 Er^{3+} transition, the longest value reported so far. The details of this work will be reported separately.[71] Another variation of the local nanostructure of Er^{3+} has produced a very efficient green up-conversion when pumped by a 980-nm laser source.[72]

III.B. Nanostructured Multiphasic Composites. The sol−gel processed multiphasic nanocomposite is an example of a system where the energy transfer between different phases can be controlled (minimized) to effect the radiative process in each domain. Since the phase separation between the different domains is on the nanometer scale, much smaller than the wavelength of light, the material is optically transparent. Such a multiphasic nanostructured composite offers the very exciting prospect of controlling excitation dynamics to derive a specific photonic response from each domain, thus achieving multifunctional activity. Taking advantage of the controlled porosity within a sol−gel prepared glass, a multiple impregnation method can be used to dope two (or more) different optically active materials in the nanopores, with each existing in different phases of the matrix.

The basic idea of a multiphasic nano-structured composite is illustrated in Figure 10. The inorganic phase (phase #1) is doped with inorganic species that can survive the heat treatment. Our processing condition[73] produces nanopores with a diameter of ∼5 nm in the glass bulk. The pores can be doped with organic functional molecules through impregnation with a solution, or by using a melt or vapor phase infiltration. After draining out the solvent and drying, the dopant organic molecules form a phase (phase #2) on the surface of the pores. Finally, the pores are filled with an index-matched polymer by in-situ polymerization of a monomer, such as methyl methacrylate. Another active organic species can also be introduced in the polymer phase (phase #3). The resultant monoliths, thus prepared, are suitable for many applications in photonics.

The multi-dye, solid-state composite glasses for tunable laser operation contain an ionic dye, (*trans*-4-[*p*-*N*-hydroxyethyl-*N*-methylamino)styryl]-*N*-methylpyridinium iodide, abbreviated ASPI), in the interfacial phase and another dye rhodamine 6G

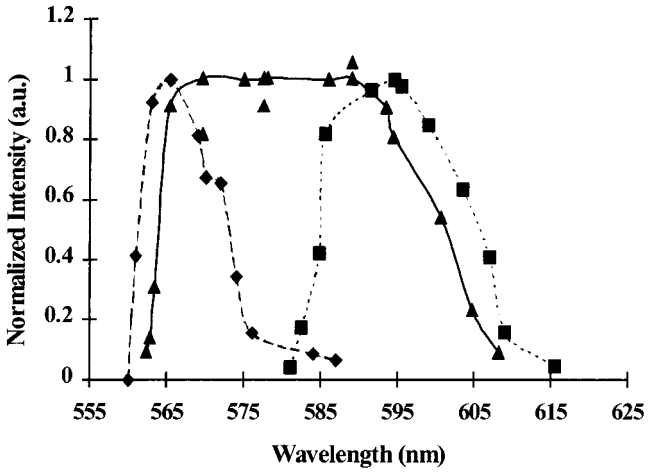

Figure 11. The lasing tunability of a multiphasic composite glass

in the polymer phase of the matrix. Lasing was observed across the regions of the individual dyes.

Figure 11 presents the lasing tunability of a multiphasic nanocomposite glass containing both dyes. Lasing tunability of the two composite glasses containing each dye separately is also shown in the same figure as a reference. The fwhm of the tunability spectra for the ASPI composite glass is ∼21 nm and that for rhodamine 6G is ∼12 nm. On the other hand, for a composite glass containing both dyes it is ∼37 nm. From these data it is evident that the laser emission from the composite glass containing both dyes is tunable across the range of both dyes, (560−610 nm), whereas in the solution state the rhodamine 6G emission is quenched. It is assumed that the quenching in the solution state is a result of Förster energy transfer. Therefore, due to the extremely large ratio between the specific surface area and the pore volume, which is $\sim 8.5 \times 10^6$, it is possible to separate the two dye molecules, (which reside in different phases) to a distance where the Förster energy transfer is considerably reduced.

III.C. Photon Localization in a Three-Dimensional Dielectric Photonic Crystals. A three-dimensional dielectric photonic crystal opens a new frontier with its focus on the experimental realization of strong localization of light and its consequences in laser physics and chemistry.[74−76] In recent years, photonic band-gap (PBG) structures have been shown to lead to the localization of light through a carefully engineered interplay between microscopic scattering resonance and coherent interference of light from many such scatterers. The basic structure of a 3D photonic crystal consists of a three-dimensional periodic arrangement of two dielectrics as shown in Figure 12. The refractive index varies at length scales on the order of optical wavelengths. The propagation of light in these materials is analogous to the well-known propagation of electrons in a crystalline structure. A photonic band gap material is a special class of photonic crystal in which a high dielectric contrast (refractive index change) exists between the two domains to provide a large scattering length. Due to the periodic structure it generates Bragg diffraction and creates a frequency band of light that cannot propagate through the crystal in any direction. Since the initial proposal of photonic band gaps, independently by John[74] and by Yablonovich,[75] PBG materials exhibiting photon localization have been fabricated at microwave frequencies.[77] More recently, large scale three-dimensional photonic crystals have been fabricated that extend from the UV to the near-infrared.[78−80] The ultimate goal for laser applications is a full three-dimensional PBG structure that can be tuned across a wide range of optical frequencies within the visible range.

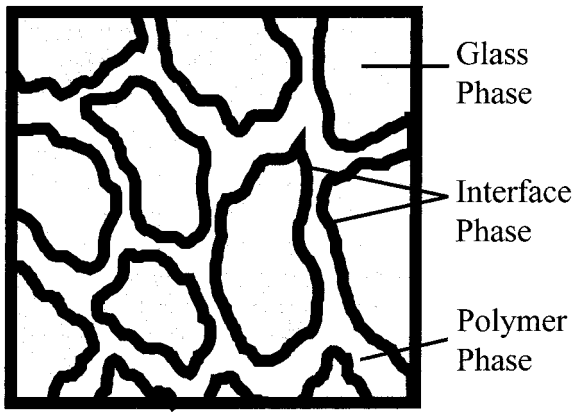

Figure 12. The photonic crystal structure of a three-dimensional periodic arrangement of two dielectrics.

A PBG material is loss-less and comprises a range of frequencies (wavelengths) for which no propagating electromagnetic modes are allowed. Therefore, atoms/molecules with transition frequencies within the gap do not experience the usual fluctuations in the electromagnetic vacuum that are responsible for spontaneous decay. Instead, a photon−atom bound state is formed. Unlike the suppression of spontaneous emission in a high-Q optical microcavity, the bound photon may tunnel many optical wavelengths away from the atom before being reabsorbed. The photon density of states is rapidly varying near a photonic band edge, making it dramatically different from the ω^2 dependence found in free space. This implies that the nature of vacuum fluctuations and thus spontaneous emission near a band edge is radically different from the exponential decay found in free space.

Although photonic band gaps are analogous to electronic band gaps in semiconductors, there are many intriguing aspects of photons that are not shared by electronic systems. Among these are laser action and super-radiance. These are related to the bosonic nature of light through which many photons can occupy the same mode. The recent observation of laser action in strongly scattering media motivates studies in this new direction.[76]

In our laboratory the growth of a photonic crystal is done through the slow sedimentation of monodisperse silica spheres at room temperature. Similar approaches using packing of silica spheres have been made by many researchers.[78,81,82] Figures 13a,b shows the SEM images of crystalline assemblies of 0.48 and 0.22 μm silica spheres, respectively. These images reveal the FCC packing at the surface and edges of the photonic crystals. Atomic force microscopy of the samples also confirmed FCC packing within the photonic crystals (Figure 14).

Optical transmission of the crystalline assemblies of 0.48 and 0.22 μm silica spheres in chloroform shows the presence of a photonic pseudogap (Figure 15, parts a and b, respectively). By varying the size of the spheres the gap can be tuned across the entire electromagnetic spectrum. It has also been shown that the photonic band gap can be thermally tuned.[83,84]

Inverted photonic crystals were prepared from TiO_2 and polystyrene (Figure 16, parts a and b, respectively). The inverted TiO_2 crystals were prepared by a method similar to Wijnhoven and Vos[81] by using polystyrene spheres and a titania precursor followed by the removal of the polystyrene spheres with heating. The inverted polystyrene was prepared through the infiltration of the silica spheres with polystyrene followed by the dissolution of the silica in HF acid. These approaches to produce photonic crystals are being used in many laboratories throughout the world.[78,81,85] The challenge is to achieve a high dielectric contrast

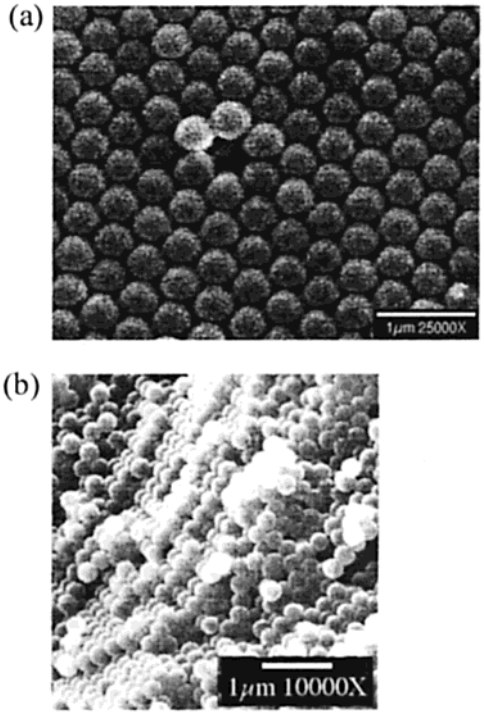

Figure 13. SEM images of crystalline assemblies of silica spheres of sizes: (a) 480 nm, (b) 220 nm.

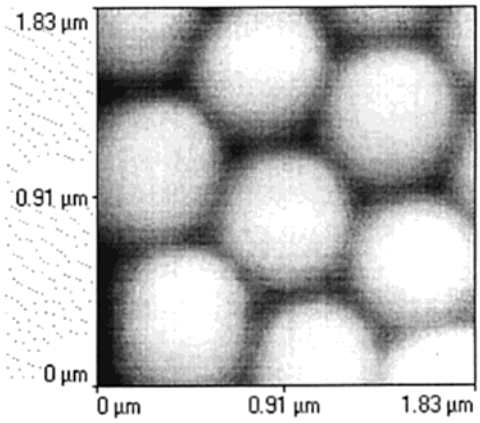

Figure 14. Atomic force microscope image of crystalline assemblies of silica spheres of 480 nm size.

(a large refractive index change) in the visible which will lead to complete photon localization. The approach that we are currently pursuing involves infiltration of silica packed microspheres with GaP using chemical vapor deposition.

IV. Applications

In our laboratory, we are pursuing a number of applications utilizing nanoscale optical processes. We are utilizing nanoscale confinement to produce photochemistry for optical data storage. Nanoscale optical storage has been carried out on magnetooptic and phase-change media recently, and data densities of 45, 2.5, and 170 Gbit/in^2 have been achieved.[54−56] But in our experiments, a spatially localized photochemical reaction, induced in a near-field geometry, is demonstrated with both one-photon and two-photon excitation on a nanometer scale and used for nanofabrication and nanoscale optical memory. The schematic diagram of the experimental setup in the present work is the same as in Figure 5a. The same self-mode-locked Ti:sapphire laser is used as the excitation source at 800 nm with an average

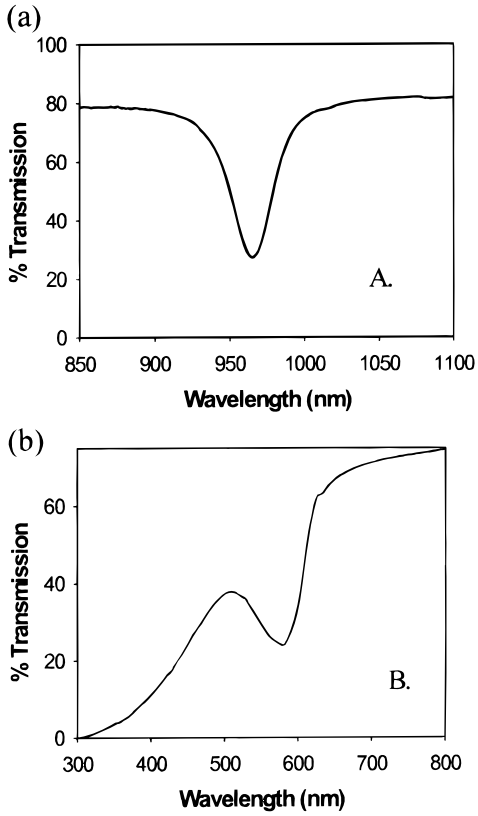

Figure 15. Optical transmission of crystalline assemblies of silica spheres of sizes: (a) 480 nm, (b) 220 nm.

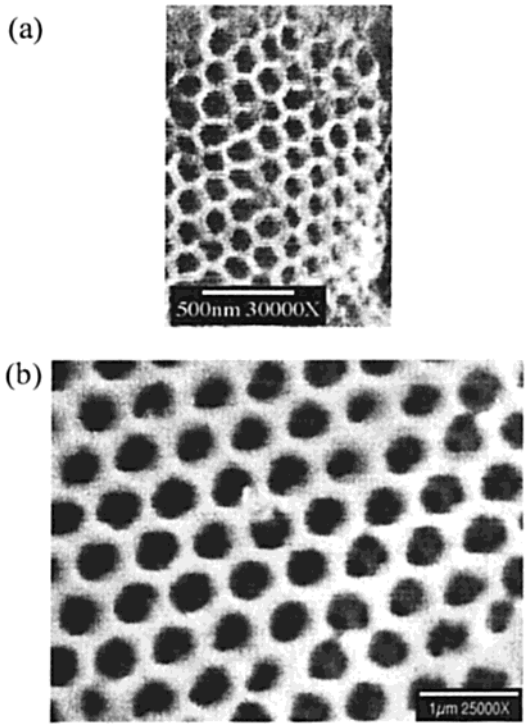

Figure 16. Inverted photonic crystals prepared from TiO_2 (a) and polystyrene (b).

power of 5.5 mW for two-photon excitation and frequency doubled at 400 nm with an average power of 3 mW for one-photon excitation. A dye-doped polymer film (AF-380/PVP) is prepared as the recording medium. Nanoscale domains result when the irradiated dyes are photobleached after being exposed for longer than 10 s. These areas show up black due to the loss of fluorescence, and are clearly distinguishable from the surrounding fluorescent areas. This difference in fluorescence intensity is easily detectable and can be used to represent 1 and 0 in recording. With one-photon excitation, we obtain a bit diameter of 120 nm, with center-to-center distance of 250 nm, as shown in Figure 17, parts a and b. Figure 18 also shows the image of the stripes recorded with one-photon excited photobleaching. The width of a written line is 130 nm, and this result implies that it is possible to fabricate nanoscale fine gratings with the near-field optical technique.

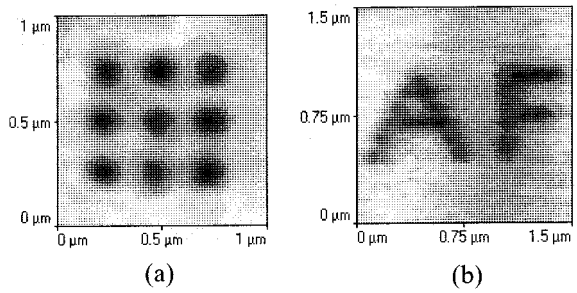

Figure 17. (a) One-photon bleached data bits, (b) The letters AF produced by one-photon bleached data bits.

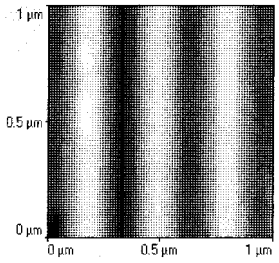

Figure 18. Fine grating structure fabricated with one-photon near-field excitation

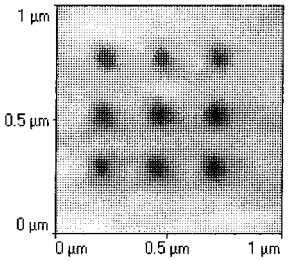

Figure 19. Near-field two-photon bleached data bits.

The spatial localization of photobleaching depends on the probe size and the intensity distribution of the local field. With one-photon excitation, photobleaching is linear and occurs in the entire zone of illumination. Consequently, relatively large data bits form. However, this can be improved by nonlinear photobleaching with two-photon excitation, because the quadratic dependence of two-photon excitation on light intensity limits the effective excitation to a small volume and enhances the local field confinement in the vicinity of the probe. With two-photon excitation, we have obtained a bit diameter of 70 nm, as shown in Figure 19.

V. Outlook for the Future

This new frontier of nanophotonics offers numerous opportunities for both fundamental research and application. Fundamental research opportunities are both for theoretical and experimental studies. Theoretical understanding of nonlinear optical processes needs to be further developed. Exciting prospects will come from an understanding of hybrid wave mixing involving both allowed and forbidden light, its spatial

distribution and polarization characteristics. Resonant wave mixing such as CARS on nanometer scale offers another theoretical opportunity. Although, linear processes in photonic crystals have been extensively analyzed, studies of nonlinear optical processes under photon localization are virtually unexplored.[86,87] Theoretical description of these processes in photonic band-gap materials will be of considerable interest.

From experimental perspectives, again the study of hybrid wave mixing is of considerable significance. Near-field probing of localized vibronic spectra using a resonant nondegenerate four-wave mixing (CARS) can detect Raman transitions on a sub-wavelength scale, and provide a better understanding of spatial and spectral dependence of CARS intensity on localized topography and environment.

From an application perspective, nonlinear near-field microscopy holds promise for high-contrast, high-resolution, and site-specific imaging. Nanofabrication and nanoscale patterning using nanoscale photochemistry will receive increasing attention.

Photonic crystals offer prospects for numerous applications: low-threshold lasing, optical-power limiting, chemical and biosensing, and optical switching. It is the sincere hope of the authors that the chemical community will play a major role in further development of this exciting field.

Acknowledgment. We thank Dr. A. Biswas and Dr. G. Maciel for their help. This work was supported by the Directorate of Chemistry and Life Science of the Air Force Office of Science Research through a University of Southern California MURI Program and in part by the Polymer Branch of the Air Force Research Laboratory at Dayton, Ohio.

References and Notes

(1) Phol, D. W.; Denk, W.; Lanz, M. *Appl. Phys. Lett.* **1984**, *44*, 651.
(2) Harootunian, H.; Betzig, E.; Isaacson, M.; Lewis, A. *Appl. Phys. Lett.* **1986**, *49*, 674.
(3) Koglin, J.; Fischer, U. C.; Fuchs, H. *Phys. Rev. B* **1997**, *55*, 7977.
(4) Birnbanm, D.; Kook, S. K.; Kopelman, R. *J. Phys. Chem.* **1993**, *97*, 3091.
(5) Xie, X. S.; Dunn, R. C. *Science* **1994**, *265*, 361.
(6) Betzig, E.; Trautman, J. K.; Harris, T. D.; Weiner, J. S.; Kostelak, R. L. *Science* **1991**, *251*, 1468.
(7) Paesler, M. A.; Moyer, P. J.; Jahncke, C. J.; Jhonson, C. E.; Reddick, R. C.; Warmack, R. J.; Ferrell, T. L. *Phys. Rev. B* **1990**, *42*, 6750.
(8) Courjon, D.; Sarayeddine, K.; Spajer, M. *Opt. Comm.* **1989**, *71*, 23.
(9) Goudonnet, J. P.; Bourillot, E.; Adam, P. M.; Defornel, F.; Salomon, L.; Vincent, P.; Neviere, M.; Ferrell, T. L. J. *Opt. Soc. Am. A* **1995**, *12*, 1749.
(10) Zhang, P.; Haslett, T. L.; Douketis, L.; Moskovits, M. *Phys. Rev. B* **1998**, *57*, 15513.
(11) Baida, F. I.; Courjon, D.; Bielefiedt, H. *Appl. Opt.* **1998**, *37*, 1808.
(12) Moers, M. H. P.; Tack, R. G.; van Hulst, N. F.; Bolger, B. *J. Appl. Phys.* **1994**, *75*, 1524
(13) Hecht, B.; Bielefeldt, H.; Novotny, L.; Heinzelmann, H. *J. Appl. Phys.* **1998**, *84*, 5873.
(14) Novotny, L. J. *Opt. Soc. Am. A* **1997**, *14*, 91.
(15) Novotny, L. J. *Opt. Soc. Am. A* **1997**, *14*, 105.
(16) Reid, P. J.; Higgins, D. H.; Barbara, P. F. *J. Phys. Chem.* **1996**, *100*, 3892.
(17) Bolton, S. R.; Bar-Ad, Sucha, S. G.; Chemla, D. S.; Sivco, D. L.; Cho, D. L. *Phy. Rev. Lett.* **1997**, *78*, 1319.
(18) Hollars, C. W.; Dunn, R. C. *J. Phys. Chem. B* **1997**, *101*, 6314.
(19) Nechay, B. A.; Siegner, U.; Genoud, F. M.; Schertel, A.; Keller, U. *Appl. Phys. Lett.* **1999**, *74*, 61.
(20) Bout, D. A. V.; Kerimo, J.; Higgins, D. A.; Barbara, P. F. *Acc. Chem. Res.* **1997**, *30*, 204.
(21) Barenz, J.; Anger, P.; Hollricher, O.; Marti, O.; Wachter, M.; Butendeich, R.; Heinecke, H. *J. Appl. Phys.* **1998**, *83*, 870.
(22) Betzig, E.; Finn, P. L.; Weiner, J. S. *Appl. Phys. Lett.* **1992**, *60*, 2484.
(23) Kopelman, R.; Tan, W. *Science* **1993**, *262*, 778.
(24) Talley, C. E.; Lee, M. A.; Dunn, R. C. *Appl. Phys. Lett.* **1998**, *72*, 2954.
(25) Rahmani, A.; Fornel, F. D. *Opt. Commun.* **1996**, *131*, 253.
(26) Weston, K. D.; Buratto, S. K. *J. Phys. Chem. B* **1997**, *101*, 5684.
(27) Hubert, C.; Levy, J. *Appl. Phys. Lett.* **1998**, *73*, 3229.
(28) Vertikov, A.; Kuball, M.; Nurmikko, A. V.; Chen, Y.; Wang, S. G. *Appl. Phys. Lett.* **1998**, *72*, 2465.
(29) Davis, R. C.; Williams, C. C. *Appl. Phys. Lett.* **1996**, *69*, 1179.
(30) Phillips, P. L.; Knight, J. C.; Mangan, B. J.; Russell, P. St.; Charlton, M. D. B.; Parker, G. J. *J. Appl. Phys.* **1999**, *85*, 6337.
(31) Smolyaninov, I. I.; Atia, W.; Davis, C. C. *Phys. Rev. B* **1999**, *59*, 2454.
(32) Hess, H. F.; Betzig, E.; Harris, T. D.; Pfeiffer, L. N.; West, K. W. *Science* **1994**, *264*, 1740.
(33) Talley, C. E.; Cooksey, G. A.; Dunn, R. C. *Appl. Phys. Lett.* **1996**, *69*, 3809.
(34) Parent, G.; Labeke, D. V.; Barchiesi, D. J. *Opt. Soc. Am. A* **1999**, *16*, 896.
(35) Smolyaninov, I. I.; Lee, C. H.; Davis, C. C. *Appl. Phys. Lett.* **1999**, *74*, 1942.
(36) Smolyaninov, I. I.; Zayats, A. V.; Davis, C. C. *Phys. Rev. B* **1997**, *56*, 9290.
(37) Bozhevolnyi, B. I.; Keller, O.; Smolyaninov, I. I. *Opt. Lett.* **1994**, *19*, 1601.
(38) Bozhevolnyi, B. I.; Geisler, T. J. *Opt. Soc. Am. A* **1998**, *15*, 2156.
(39) Jakubczyk, D.; Shen, Y.; Lal, M.; Friend, C.; Kim, S. K.; Swiatkiewicz, J.; Prasad, P. N. *Opt. Lett.* **1999**, *16*, 1151.
(40) Shen, Y.; Jakubczyk, D.; Xu, F.; Swiatkiewicz, J.; Prasad, P. N.; Reinhardt, B. A. *Appl. Phys. Lett.* **2000**, *76*, 1.
(41) Vigourenx, J.; Girard, M. C.; Depasse, F. J. *Mod. Opt.* **1994**, *41*, 49.
(42) Lewis, M. K.; Wolanin, P.; Gafni, A.; Steel, D. G. *Opt. Lett.* **1998**, *23*, 1111.
(43) Hell, S. W.; Booth, M.; Wilms, S.; Schnetter, C. M.; Kirsch, A. K.; Arndt-Jovin, D. J.; Jovin, T. M. *Opt. Lett.* **1998**, *23*, 1238.
(44) Zhao, X.; Kopelman, R. *Ultramicroscopy* **1995**, *61*, 69.
(45) Kumar, N. D.; Lal, M.; Prasad, P. N. *Science and Technology of Polymers and Processing of Multifunctional Polymers and Composites for Photonics*; Plenum Press: New York, 1998.
(46) Romanov, S. G.; Maka, T.; Torres, C. M. S.; Muller, M.; Zentel, R. *Appl. Phys. Lett.* **1999**, *75*, 1057.
(47) Paspalakis, E.; Keitel, C. H.; Knight, P. L. *Phys. Rev. A* **1998**, *58*, 4868.
(48) Lin, S. Y.; Fleming, J. G.; Sigalas, M. M.; Biswas, R.; Ho, K. M. *Phys. Rev. B.* **1999**, *59*, 15579.
(49) Miyazak, H.; Ohtaka, K. *Phys. Rev. B.* **1998**, *58*, 6920.
(50) Chan, Y. S.; Chan, C. T.; Liu, Z. Y. *Phys. Rev. Lett.* **1998**, *80*, 956.
(51) Russell, P. S.; Roberts, P. J.; Allan, D. C. *Science* **1999**, *285*, 1537.
(52) Herndon, M. K.; Collins, R. T.; Hollingsworth, R. E.; Larson, P. R.; Johnson, M. B. *Appl. Phys. Lett.* **1999**, *74*, 141.
(53) Nolte, S.; Chichkov, B. N.; Welling, H.; Shani, Y.; Lieberman, K.; Terkal, H. *Opt. Lett.* **1999**, *24*, 914.
(54) Betzig, E.; Trautman, J. K.; Wolfe, R.; Gyorgy, E. M.; Finn, P. L. *Appl.* Phys. *Lett.* **1992**, *61*, 142.
(55) Terris, B. D.; Mamin, H. J.; Rugar, D. *Appl. Phys. Lett.* **1996**, *68*, 141.
(56) Hosaka, S.; Shintani, T.; Miyamoto, M.; Hirotsune, A.; Terao, M.; Yoshida, M.; Fujita, K.; Kammer, S. *Jpn. J. Appl. Phys.* **1996**, *35*, 443.
(57) Tan, W.; Shi, Z. Y.; Smith, S.; Birnbaum, D.; Kopelman, R. *Science* **1992**, *258*, 778.
(58) Hafner, C.; Bomhddt, L. H. *The 3d Electrodynamic Wave Simulator*; Wiley: Chichester, U.K., 1993.
(59) Novotny, L.; Pohl, D. W.; Regli, P. *J. Opt. Soc. Am. A* **1994**, *11*, 1768.
(60) Shen, Y. R. *The Principles of Nonlinear Optics*; Wiley: New York, 1984.
(61) Andreazza, P.; Josse, D.; Kfaucheux, F.; Robert, M. C.; Zyss, J. *Phys. Rev.* **1992**, *B45*, 7640−7649.
(62) Denk, W.; Strickler, J. H.; Webb, W. W. *Science* **1990**, *248*, 73.
(63) Sanchez, E. J.; Novotny, L.; Xie, X. S. *Phys. Rev. Lett.* **1999**, *82*, 4014.
(64) Betzig, E.; Chichester, R. J. *Science* **1993**, *262*, 1422.
(65) Trautman, J. K.; Mavklin, J. J.; Brus, L. E.; Betzig, E. *Nature* **1994**, *369*, 40.
(66) Bout, D. A. V.; Kerimo, J.; Higgins, D. H.; Barbara, P. F. *J. Phys. Chem.* **1996**, *100*, 11843.
(67) Fornel, F.; Salomon, L.; Adam, P.; Bourillot, E.; Goudonnet, J. P. *Ultramicroscopy* **1992**, *42*, 422.
(68) Weisbuch, C.; Benisty, H.; Houdre, R. *J. Lumin.* **2000**, *85*, 271.
(69) Lal, M.; Kumar, N. D.; Joshi, M. P.; Prasad, P. N. *Chem. Mater.* **1998**, *10*, 1065.
(70) *MRS Bulletin* **1999**, *24* (9).
(71) Biswas, A.; Maciel, G. S. To be published.
(72) Kapoor, R.; Friend, C. S.; Biswas, A.; Prasad,P. N. *Opt. Lett.* **2000**, *25*, 338.

(73) Ruland, G.; Gvishi, R.; Prasad P. N. *J. Am. Chem. Soc.* **1996**, *118*, 2985.
(74) John, S. *Phys. Rev. Lett.* **1987**, *58*, 2486.
(75) Yablonovich, E. *Phys. Rev. Lett.* **1987**, *58*, 2059.
(76) Yamamoto, Y.; Slusher, R. E. *Phys. Today* **1993**, *46(6)*, 66.
(77) Rowson, S.; Chelnokov, A.; Lourtioz, J. M. *J. Lightwave Technol.* **1999**, *17*, 1989.
(78) Xia, Y. N.; Gates, B.; Park, S. H. *J. Lightwave Technol.* **1999**, *17*, 1956.
(79) Fink, Y.; Urbas, A. M.; Bawendi, M. G.; Joannopoulas, J. D.; Thomas, E. L. *J. Lightwave Technol.* **1999**, *17*, 1963.
(80) Zakhidov, A. A.; Baughman, R. H.; Iqbal, Z.; Cui, C. X.; Khayrullin, I.; Dantas, S. O.; Marti, I.; Ralchenko, V. G. *Science* **1998**, *282*, 897.
(81) Wijnhoven, J. E. G. J.; Vos, L. V. *Science* **1998**, *281*, 802.
(82) Subramania, G.; Constant, K.; Biswas, R.; Sigalas, M. M.; Ho, K. M. *Appl. Phys. Lett.* **1999**, *74*, 3933.
(83) Pan, G.; Kesavamoorthy, R.; Asher, S. A. *J. Am. Chem. Soc.* **1998**, *120*, 6525.
(84) Ballato, J.; James, A. *J. Am. Ceram. Soc.* **1999**, *82*, 2273.
(85) Miguez, H.; Blanco, A.; Lopez, C.; Meseguero, F.; Yates, H. M.; Pemble, M. E.; Lopez-Tejeira, F.; Garcia-Vidal, F. J.; Sanchez-Dehesa, J. *J. Lightwave Technol.* **1999**, *17*, 1975.
(86) John, S.; Busch, K. *J. Lightwave Technol.* **1999**, *17*, 1931.
(87) Pan, G.; Kesavamoorthy, R.; Asher, S. A. *Phys. Rev. Lett.* **1997**, *78*, 3860.